ORIGINAL ARTICLE

Research on the sidewall penetration mechanisms of cable-type welding wire narrow gap GMAW process

Zhidong Yang[1] · Yuntao Chen[1] · Zewei Zhang[1] · Chenfu Fang[1] · Kai Xu[2] · Peng He[3] · Zhengdong Zhang[1]

Abstract

A method of narrow gap gas metal arc welding (NG-GMAW) with a self-rotating arc was established using cable-type welding wire. The wire melting speed, metal deposition, and welding seam thermal cycles of cable-type welding wire (CWW) GMAW and single-wire GMAW at the same welding parameters were studied and analyzed. The microstructural characteristics and mechanical properties of the weld were analyzed. The results showed that CWW was highly efficient and exhibited satisfactory sidewall penetration in the welding process. With its special structure, the surface area and the heating provided by the electrical resistance of CWW were distinctly higher than those of the single wire, thus resulting in CWW GMAW exhibiting higher efficiency than single-wire GMAW. The sidewall penetration of CWW NG-GMAW was analyzed in terms of arc rotation, droplet transfer motion, and regular molten pool flow. The combination of the arc rotating force and droplet transfer force on the molten pool promoted heat transfer to both sidewalls, affecting the features of the sidewall and the bottom width of the molten pool.

Keywords GMAW · Cable-type welding wire · Arc rotation · Sidewall penetration · Narrow gap welding

1 Introduction

Thick plates are more widely used in modern production with the mature development of manufacturing large structural parts, and narrow gap welding has numerous applications in a variety of industrial manufacturing fields [1, 2]. Many methods, such as electron beam welding, laser welding, and friction stir welding, have been proposed to enhance the welding efficiency and obtain good sidewall penetration in the narrow gap when welding thick plates [3–5]. Each of these methods has advantages in terms of the weld quality, efficiency, and low consumption of materials; however, these methods need special welding environments and specific

working positions while also exhibiting complex mechanics and a high cost [6].

The gas metal arc welding (GMAW) method is still a popular welding method that is applied in narrow gap welding; thus, most studies are focused on this method and related methods. Wang et al. [7] adopted a hollow axis motor-driven high-speed rotating arc system for narrow gap welding, which could improve the penetration into groove sidewalls and the bead shape. Guo et al. [8] developed a rotating arc system to solve the sagging problem of the molten pool due to gravity, in which the synchronous motor-driven rotation of the nozzle and wire was generated by an eccentric sleeve. This welding process reduced the effective heat input during welding and dispersed the arc force to counteract the gravity of the upper side of the molten metal. Cui et al. [9] developed a swing arc welding system for horizontal narrow gap welding in heavy plate structures, and this system could achieve complete sidewall penetration and high tensile properties. Xu et al. [10] proposed a three-dimensional unified model to simulate the molten pool dynamic behavior in swing arc narrow gap vertical GMAW and investigated the weld formation mechanism of swing arc vertical-up welding.

Many methods used to reduce narrow gap GMAW (NG-GMAW) defects, such as preheating and oscillation, are

✉ Zhidong Yang
yangzhidong@just.edu.cn; 13952846832@163.com

1 College of Materials Science and Engineering, Jiangsu University of Science and Technology, Zhenjiang 212003, China

2 Harbin Welding Institute Limited Company, Harbin 150028, China

3 College of Materials Science and Engineering, Harbin Institute of Technology, Harbin 150006, China

Fig. 1 Photograph and schematic illustrations of the CWW. (**a**) Product picture. (**b**) Schematic of the 7-wire CWW
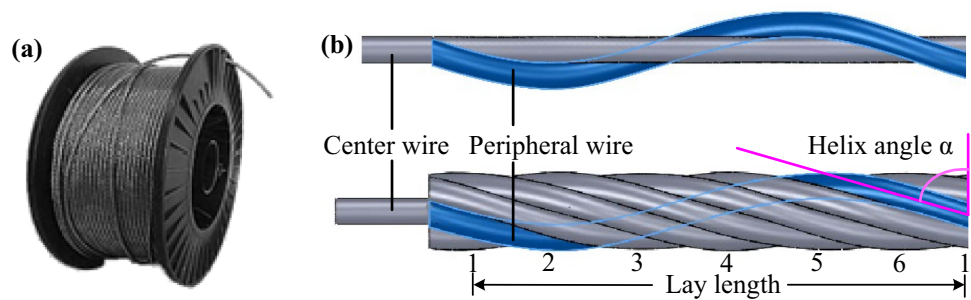
effective measures for controlling welding defects. Jones et al. [11] proposed tandem gas metal arc welding with the ends of the contact tips were bent to direct the arcs toward opposite sidewalls to increase the sidewall penetration. Cai et al. [12] used different shielding gas in tandem narrow gap gas metal arc welding, obtaining the largest weld width with the shielding gas mixture of 80%Ar, 10%CO_2, and 10%He. Zhu et al. [13] combined a preheating and oscillating arc process for narrow-groove butt joint welding, obtaining a defect-free weld joint in a section of a thick aluminum alloy. In this method, the heat-affected zone (HAZ) was enlarged, and a greater number of equiaxed grains grew in the weld bead with an increase in preheating temperature. Li et al. [14] established a variable groove model with arc sensing and visual sensing to predict sidewall penetration by the welding current and shortest distance between the arc center and the groove sidewall.

Sidewall fusion is one of the main problems and is also a key issue that needs to be solved during narrow gap gas metal arc welding [15, 16]. To simplify the assisting equipment, a CWW NG-GMAW method has been proposed. The CWW is composed of 7 single wires, with one in the center and the other six distributed uniformly around it with a helix angle [17, 18]. To prove the feasibility of CWW NG-GMAW, this paper studies the wire melting speed, deposition speed, energy consumption, and narrow gap welding process using cable wire and analyzes the behavior and high efficiency of sidewall melting. Thus, a theoretical foundation basis for the application of cable wire gas in a narrow gap process is established.

2 Experimental materials and method

2.1 Experimental materials

The wire used for CWW NG-GMAW is shown in Fig. 1. A single wire and CWW were used with a diameter of 2.4 mm

(Φ2.4) as filler metal, as shown in Fig. 1a. The CWW was composed of 7 wires: one was in the center and the other six were distributed around the central wire as shown in Fig. 1b. Both types of wire were YL-ER50-6. Q345B was used as workpieces. Details of the chemical composition of the wire and filler metal details are shown in Table. 1. The steel plates with dimensions of 400 mm × 150 mm × 10 mm were used as butt joint base metal. The details of the weld joint assembly and butt joint shape are shown in Fig. 2.

2.2 Experimental method and parameters

A schematic of the CWW NG-GMAW system is shown in Fig. 3 and the welding system mainly consists of a welding power source, welding torch, wire feed motor, CWW, and shielding gas. The quality analyzer, high-speed camera synchronous system, contact thermocouples, and data recorder were used for data collection during the welding process. The workpieces moved with the platform, while the torch remained still. The CWW was driven by a wire feed motor, and the CWW rotation speed was affected by the wire feed speed and helix angle. The temperature between layers is 100 ± 10 °C, and the welding parameters are shown in Table 2. The shielding gas was 82% Ar + 18% CO_2 at a flow rate of 30 L/min. A 10 mm × 10 mm × 55 mm V-notch specimen was used to test for impact performance. The bending experiment was carried out at a bending angle of 180°.

3 Results and discussion

3.1 Melting and deposition

The melting and deposition speeds of Φ2.4 mm CWW GMAW and Φ2.4 mm single-wire GMAW are shown in Fig. 4. The wire melting speed and deposition speed

Table 1 Chemical composition of the wire and base metal

Material	C	Mn	Si	S	P	Cr	Ni	Mo	Cu	V
Wire	0.18	1.40	0.97	0.013	0.013	0.018	0.0001	0.0001	0.019	0.0001
Base metal	≤0.20	≤1.70	≤0.50	≤0.035	≤0.035	≤0.30	≤0.50	≤0.10	≤0.30	≤0.15

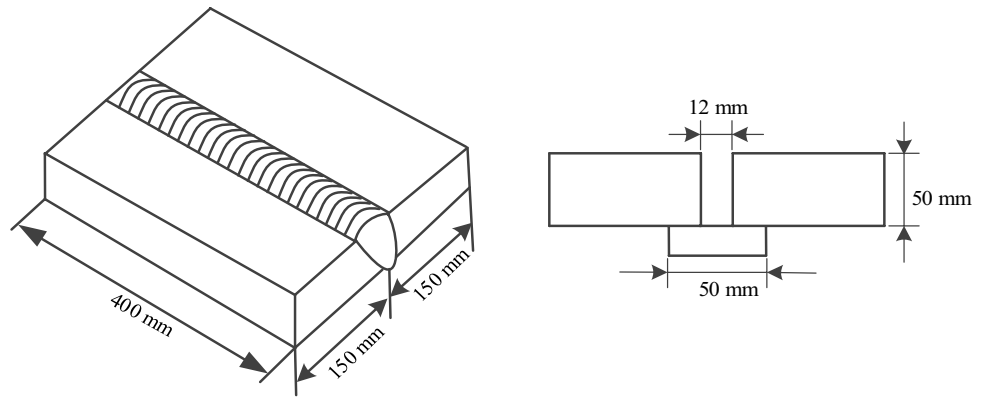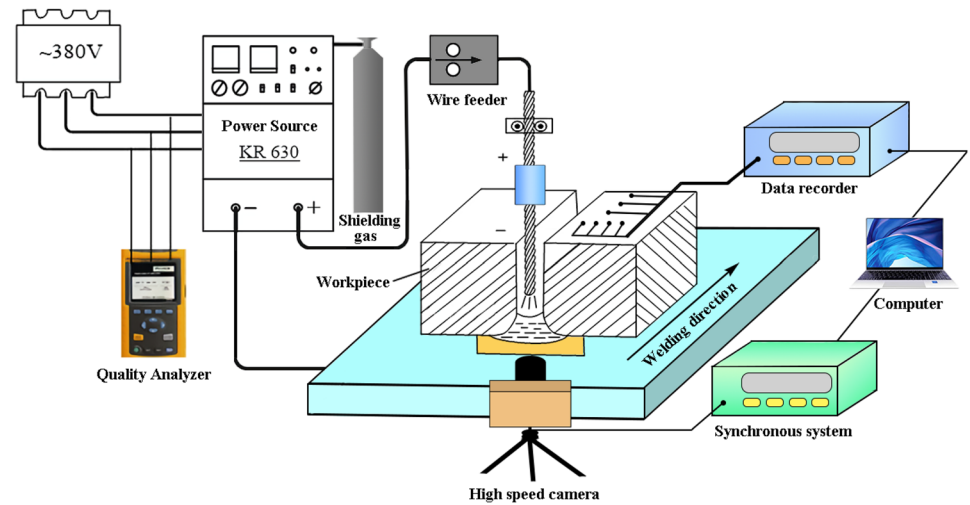**Fig. 2** Butt joint assembly and shape

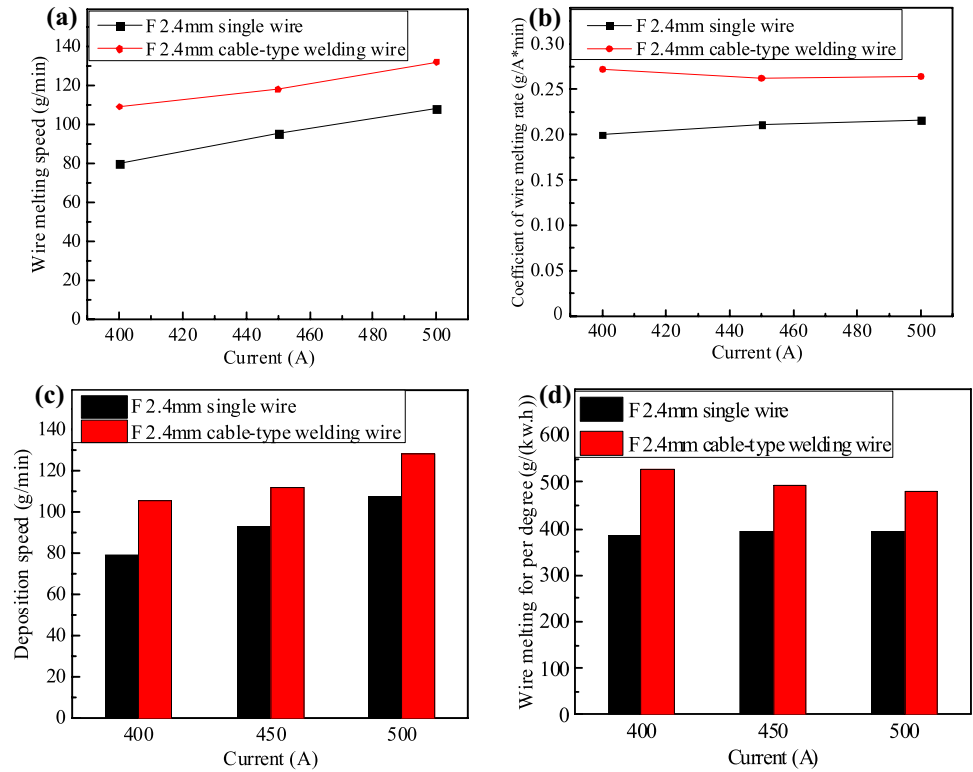
Fig. 3 Schematic of the CWW NG-GMAW system

change as the current increases. Flat plate surface welding was used to compare the two welding processes, and it is found that the 2.4 mm CWW melting speed was approximately 21% higher than that of the single wire with the same welding process parameters. The melting speed and deposition speed of both methods increase with an increasing current, and the melting speeds of the CWW and single wire reach their maximum values at welding parameters of 500 A and 33 V, as shown in Fig. 4a. The coefficient of the wire melting speed and deposition speed of the CWW is 24.5% higher than that of the single wire (2.4 mm). The deposition speed of single-wire GMAW and CWW GMW increase with the current, while the melting coefficient has less effect compared with the deposition speed, as shown in Fig. 4b–c. The weight of the deposited CWW at 1 kWh is 27.5% higher than that of a single wire (welding parameters of 400 A and 31 V), as shown in Fig. 4d.

Table 2 Parameters of the CWW NG-GMAW process

Process	Experiment number	Welding current (I), A	Welding voltage (U), V	Wire extend (L), mm	Welding speed (V), cm/min
CWW GMAW (Φ2.4 mm)	No. 1	420	32	35	25
	No. 2	460	33	25	22
	No. 3	460	33	25	22
	No. 4	460	33	25	22
	No. 5	460	33	25	22
	No. 6	460	33	25	22
	No. 7	420	32	25	20

3.2 Weld morphology

The cross-section of the CWW NG-GMAW multilayer weld formation is shown in Fig. 5. The CWW NG-GMAW process is stable, and the ray detection results show no internal defects, such as pores, cracks, lack of penetration, incomplete fusion, and striped slags, in the docking plate welds, as shown in Fig. 5a. In addition, the sidewall melting depth on both sides of the workpieces meets the requirements, as shown in Fig. 5b. A schematic of different areas of the CWW NG-GMAW butt joint is shown in Fig. 6. The butt joint contains the base metal, fusion zone, interface between the fusion and the weld zone, HAZ, weld zone, and junction between two welds.

3.3 Welding seam thermal cycles

The welding seam thermal cycles of a CWW and single-wire weld seam are shown in Fig. 7. A distribution of featured points was applied to measure temperature during single-wire GMAW and CWW GMAW, as shown in Fig. 7a. The temperature change law of CWW and single-wire GMAW at the same test point position is similar for the same welding parameters, while the maximum temperature is different, as shown in Fig. 7b, c. The temperature gradually increases during the heating of the arc, and then, the temperature gradually shows a downward trend. However, the temperature on the outside of the weld seam with CWW GMAW is

Fig. 5 Cross-section of the formed weld with CWW NG-GMAW. (**a**) Weld shape. (**b**) Cross-section of the weld seam
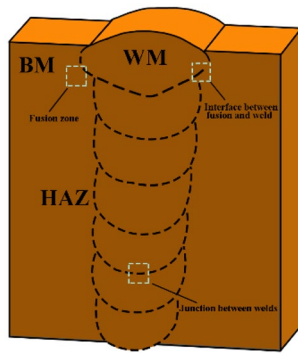
Fig. 6 Schematic showing the sampling method of a multipass welded specimen

higher than that with single-wire GMAW because CWW can transfer more energy away from the weld.

3.4 Microstructure and processing properties of the weld joints

The microstructures of the different areas of the CWW NG-GMAW sample are shown in Fig. 8. As shown in Fig. 8a−f, coarse grains and fine grains exist in different areas from the weld to the base metal. The fusion zone is the junction zone between the weld and the base metal, which is the transition zone from the weld metal to the heat-affected zone in the welded joint. The microstructure of the fusion zone is smaller than that of the weld zone, as shown in Fig. 8b. Between the weld zone and the HAZ is a junction zone,
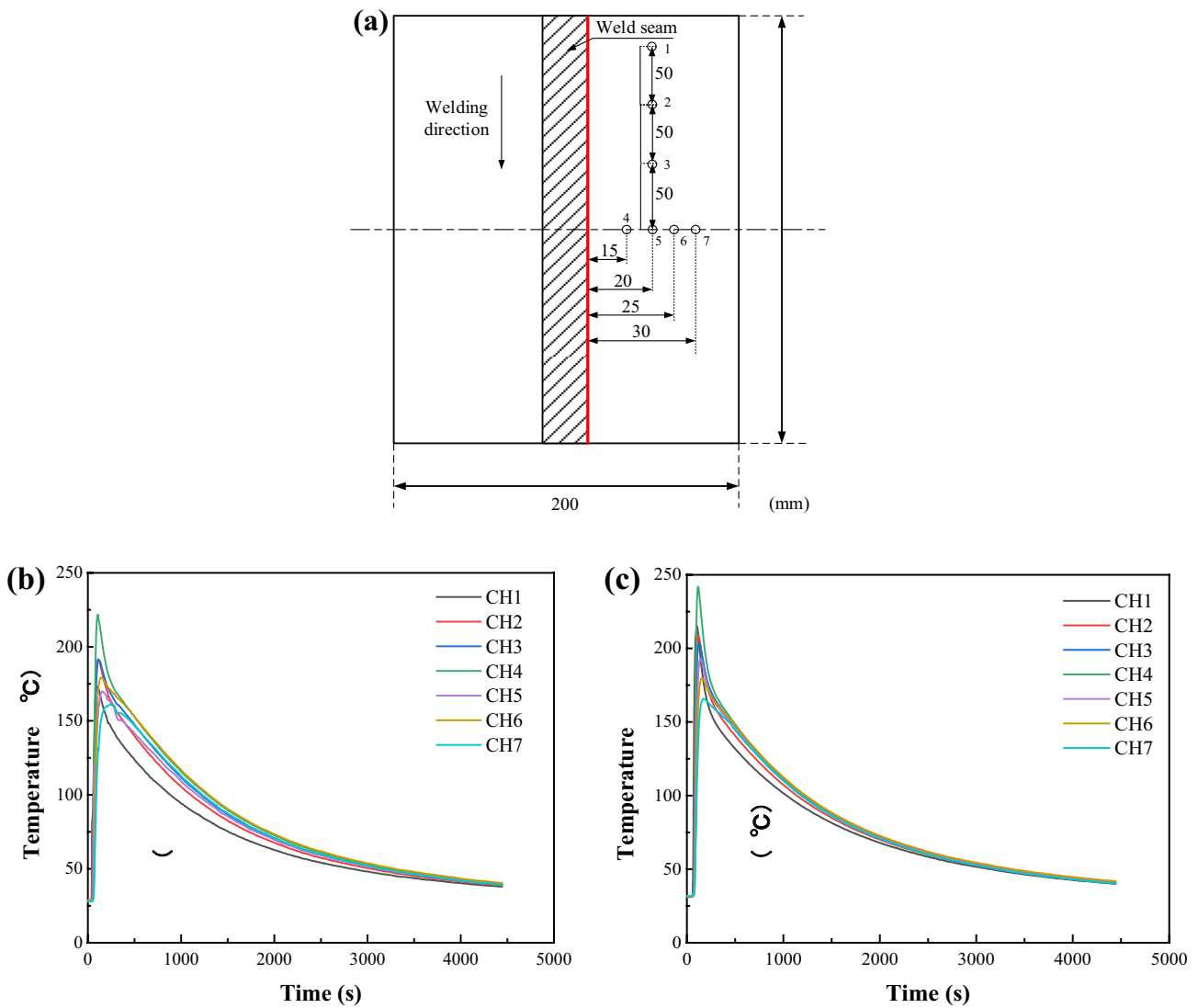

Fig. 7 Welding seam thermal cycles. (**a**) Distribution of featured points. (**b**) Single-wire GMAW. (**c**) CWW GMAW

and the microstructure of the weld zone and fusion zone is shown in Fig. 8c. The microstructures of the weld zone and HAZ are coarse grains, and these grains are larger than those in other parts of the weld, as shown in Fig. 8d, e. In the junction zone, the microstructure is a mixture of coarse grains and fine grains that form by the heat effect of the next welding pass, as shown in Fig. 8f.

Through tensile, bend, and impact tests, it is found that CWW NG-GMAW meets the China Classification Society (CCS) standard requirements. The tensile experiment of the CWW NG-GMAW sample is shown in Fig. 9. The fracture positions of the two workpiece samples are located far from the weld seam. The tensile test result shows that the weld seam tensile strength is similar to that of the workpieces and can meet the use requirements, as shown in Table 3. The side bend test of the CWW NG-GMAW sample shows no cracks or other defects, as shown in Table 4.

The impact test results of the CWW NG-GMAW sample are shown in Table. 5. All the Charpy V notched impact test results meet the ship welding requirement at room temperature [19]. The results in the HAZ are lower than the results at the seam center and fusion line, which is similar to normal welding in the flat position. The HAZ is the weakest area of a weld joint, which is the junction of the weld and workpieces. Therefore, the CWW NG-GMAW demonstrates welds with good toughness.
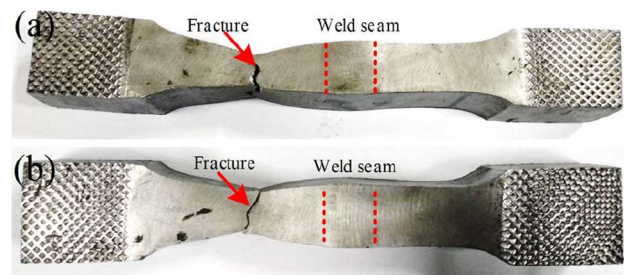

Fig. 9 Tensile experiment of the CWW NG-GMAW sample. (**a**) Sample 1. (**b**) Sample 2

The hardness test results of the CWW NG-GMAW sample at a distribution of points along the cross-section of the welding seam are shown in Fig. 10. The weld hardness value is less than 355 HV, which meets the requirement of the CCS standard. The hardness trends at the top, center, and bottom of the weld are similar, and the hardness at the center and bottom of the weld are higher than that at the top. The reason for this result is that the bottom and center welds are heated by the heat of the next weld, which can increase the weld hardness value [20, 21]. As the heat from the arc gradually decreases from the center of the weld to both sides, the temperature at the center is higher than that at both sides of the weld, and the rapid cooling during the cooling process causes the hardness value of the center of the weld to show the above phenomenon.
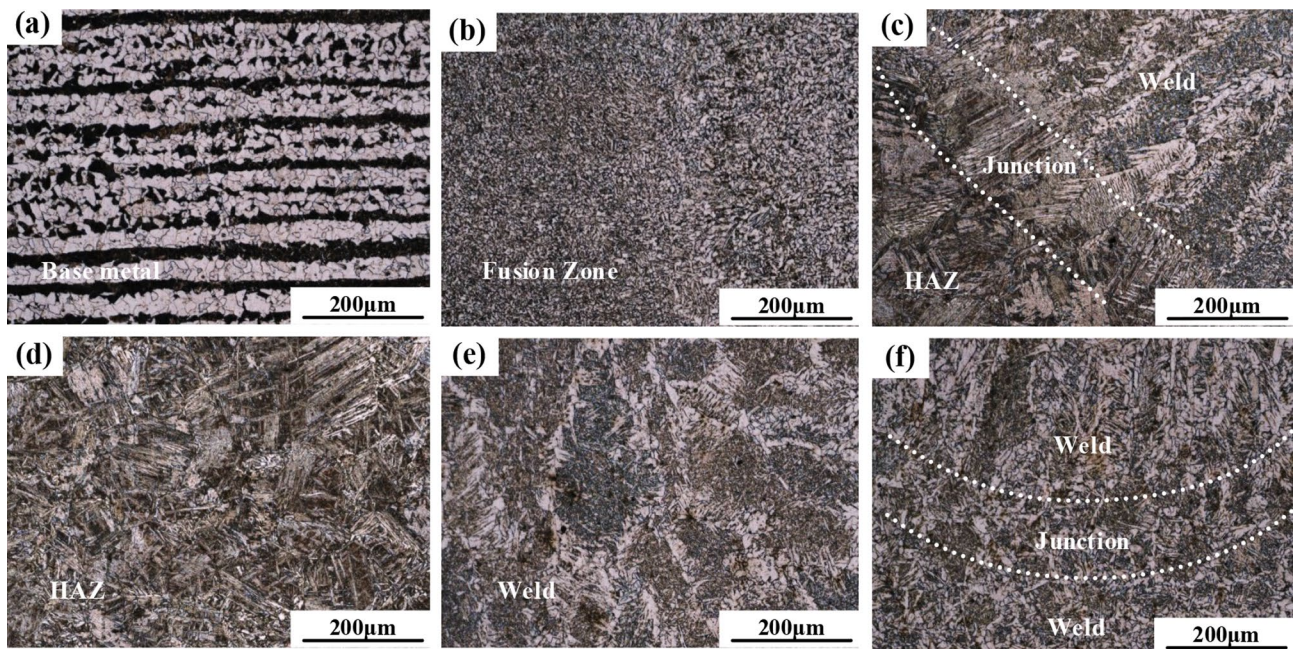

Fig. 8 Microstructures of CWW NG-GMAW weld. (**a**) Base metal. (**b**) Fusion zone. (**c**) Interface between fusion and weld. (**d**) HAZ, (**e**) Weld zone. (**f**) Junction between welds

Table 3 Result of the tensile test

Weld method	Sample number	Cross-sectional area, mm	Maximum load, kN	Tensile strength, MPa	Fracture position
CWW NG-GMAW	1	25 × 29.9	386	516	Base metal
	2	25 × 30.1	392	520	Base metal

Table 4 Results of the side bend test

Method	Number	Result
CWW NG-GMAW	11, 12, 13, 14	No crack

Table 5 Results of the impact test

Process	Number	Position	A_{kv} (20 °C) Average, J
CWW NG-GMAW	1/2/3	Seam center	97
	4/5/6	Fusion line	83
	7/8/9	HAZ	52

3.5 Mechanism of NG-CWW GMAW

In narrow gap welding, sidewall melting is the key problem that needs to be solved. CWW NG-GMAW can achieve sidewall melting and high-efficiency welding, and the high efficiency and sidewall melting mechanism are mainly related to the motion of the arc, drop motion trajectory, and molten pool flow characteristics.
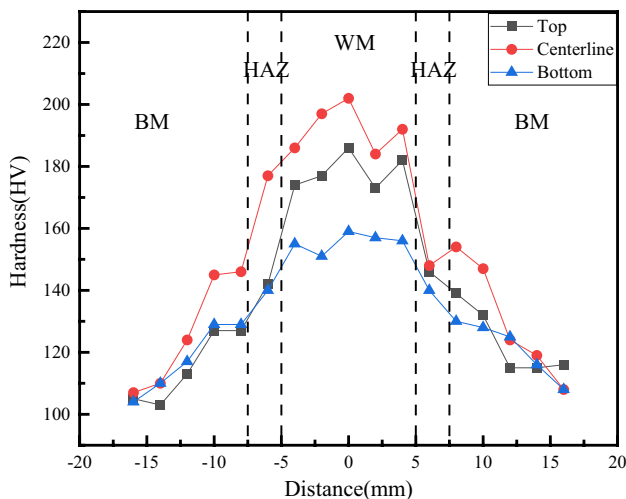

Fig. 10 Hardness test results of the CWW NG-GMAW sample at a distribution of points along the cross-section of the welding seam

3.5.1 High-efficiency welding mechanism

The energy in the welding process is mainly composed of arc heat and resistance heat [22]. It is assumed that the CWW and single wire generate the same arc heat at the same welding parameters when they have the same diameter. Therefore, the heat generated and heat absorption of the welding wire in the two welding processes were analyzed.

1. Surface area

   The CWW used in this experiment is made up of 7 wires, and this structure is different from the structure of a single wire. Therefore, the surface area between the CWW and single wire is also different. Depending on the structure of the wire, the surface areas can be represented by the following formulas.
   The surface area of CWW can be expressed as

$$S_w = 7 \times 2\pi r(r + h) \tag{1}$$

   The surface area of the single wire can be expressed as

$$S_s = 2\pi r(r + h) \tag{2}$$

where S_w is the surface area of CWW, S_s is the surface area of a single wire, r is the radius of CWW, h is the height of the welding wire.

By comparing Eqs. (1) and (2), it can be found that the surface area of CWW is 4.6 times (S_w/S_s) higher than that of a single wire at the same diameter. The CWW is formed by stranding multiple fine wires, and each wire has its own surface area. Therefore, the surface area of CWW is larger than that of a single wire. It is assumed that the CWW arc heat is the same as the arc heat generated by the single wire at the same welding parameters, despite the surface contact area of CWW with the arc is larger than that of the single wire with the arc. Thus, the CWW more easily absorbs the heat of the arc than that of a single wire during the welding process, which can increase the amount of melted wire. Therefore, the melting efficiency of CWW is higher than that of the single wire under the same conditions, and this result is consistent with the comparison between the CWW and single-wire melting efficiency when both materials have the same diameter.

Fig. 11 Arc shape of CWW and single-wire GMAW. (**a**) CWW GMAW. (**b**) Single-wire GMAW
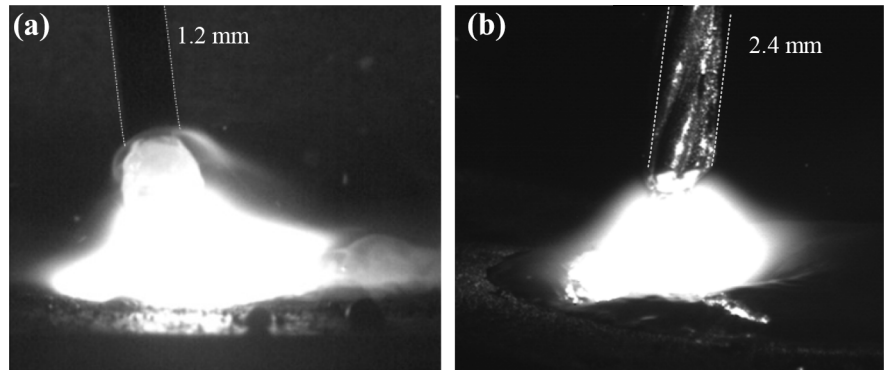
2. Resistance heat

The melting process of welding wire is related to many factors during the welding process, such as the welding parameters, wire polarity, wire diameter, weld wire composition, weld wire surface shape, and protective media. The heat used to melt the wire is mainly composed of arc heat and resistance heat during the GMAW process. The resistance of the welding circuit is composed of the resistance of the arc, wire extension, and other internal components [23, 24]. Therefore, the energy required to melt the CWW is expressed as

$$Q_m = \eta_1 I [U - I(R_w + R_0)] t + \eta_2 I^2 R_w t \tag{3}$$

where Q_m is the energy to melt CWW, η_1 is the thermal efficiency coefficient of arc heat, I is the welding current, U is the welding voltage, t is the welding time, R_w is the resistance of the CWW extension, R_0 is the total internal resistance of the welding circuit, and η_2 is the thermal efficiency coefficient of resistance heat.

The single-wire GMAW resistance could describe as the formula (4) according to the principle of arc welding.

The resistance of CWW is composed of the actual length of resistance and the variable resistance with parallel connection. The variable resistance is related to the wire diameter, spiral angle, and number of wires. Assuming that the spiral angle $\alpha = 30^\circ$ and that the wire extension is L, the external wire length can be described as $2\sqrt{3}L/3$. Therefore, the resistance of CWW could describe by formula (5):

$$R_s = \rho \frac{L}{\pi(1.2)^2} \tag{4}$$

$$R_w = \frac{\sqrt{3}}{1 + 3\sqrt{3}} \rho \frac{L}{\pi(0.4)^2} \tag{5}$$

where R_s is the resistance of a single wire, ρ is the wire resistivity, L is the wire extension, and R_c is the total resistance of CWW.

The sum of the effective heat of the arc heat and the resistance heat should be greater than the energy required to melt the welding wire if the welding wire is completely melted. Assuming $R_0 = 0$, the melting speed of a single wire and CWW in the case of certain welding conditions and welding materials can be expressed as:

Fig. 12 Schematic illustration showing the arc rotation and trajectory of motion
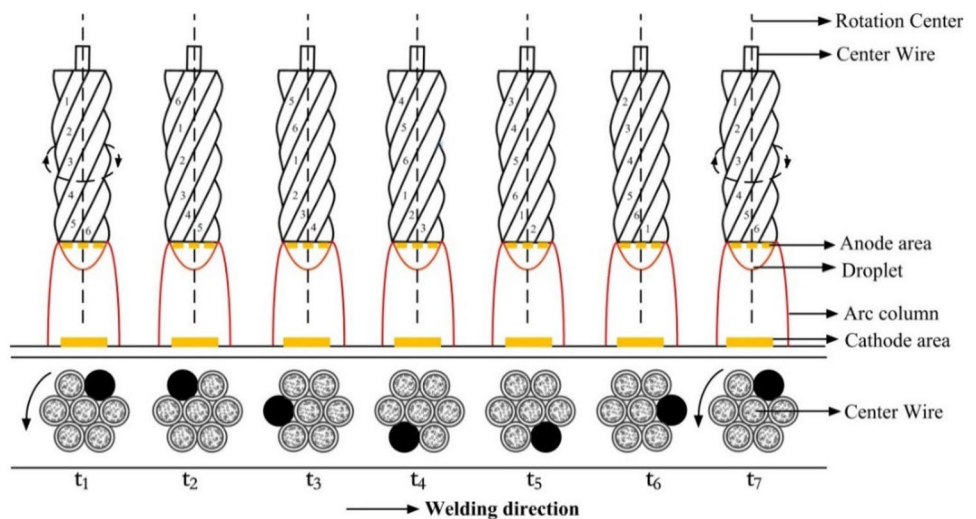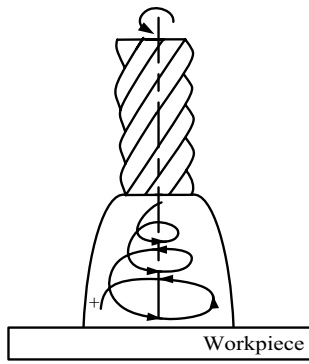
Fig. 13 Diagram of charged particle motion under a mechanical rotation force

$$v_w = \frac{\eta_1 IU + 0.69I^2 \rho \frac{L}{\pi r^2}(\eta_2 - \eta_1)}{C\Delta T_w} \tag{6}$$

$$v_s = \frac{\eta_1 IU + I^2 \rho \frac{L}{\pi r^2}(\eta_2 - \eta_1)}{C\Delta T_s} \tag{7}$$

where v_c and v_s are the CWW melting speed and single-wire melting speed, respectively. C is the wire specific heat capacity, ΔT_w is the temperature difference of the CWW from the heating to the melting phase transition, and ΔT_s is the temperature difference of the single wire from the heating to the melting phase transition,

It is assumed that the arc, resistance thermal efficiency coefficient, welding wire ratio thermal capacity, and welding wire temperature difference from heating to transition are the same. These formulas show that the resistance of the CWW can produce approximately 1.45 times (v_w/v_s) more heat than a single wire under the same welding conditions and wire diameter. That is, the CWW could produce more heat than that of a single wire along the same amount of wire extend. This result is beneficial for the melting, droplet formation, and droplet growth of CWW; thus, CWW demonstrates an
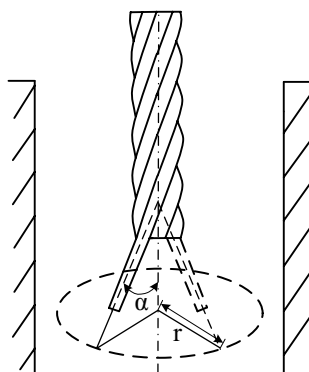
enhanced wire melting rate. Additionally, the consumption of electrical energy by CWW GMAW is lower than that of single-wire GMAW with the same deposition of melted wire, and this result is consistent with the law of change of CWW and single-wire melting, as shown in Fig. 4.

By analyzing the surface area and resistance heat of each wire, it can be found that the absorption of heat (due to surface area) and production of heat (due to resistance) of the CWW are greater than that of the single wire under the same welding conditions. Thus, the CWW is more beneficial for improving the melting speed and melting efficiency during the welding process, and this result is consistent with the test results.

3.5.2 Sidewall penetration behavior

Sidewall penetration is an important problem that needs to be solved in NG-GMAW. The sidewall penetration of CWW NG-GMAW is mainly related to the arc rotation, metal transfer, and melting pool flow; the aspects of these parameters are analyzed below.

1. Arc rotation features

The arc shapes of CWW GMAW and single-wire GMAW are shown in Fig. 11. The arc is at the end of CWW, and the shape is similar to a bell. The phenomenon of the CWW GMAW arc shape interaction and coupling can be explained by the deflection length model [25], which states that the current running through the individual wires makes a concentrated force at the center wire. Due to the special structure of the CWW, the position of the wire changes relatively with continuous wire delivery during CWW GMAW, as shown in Fig. 12. From the wire tip of the CWW, it can be seen that the wire will rotate as the wire is fed by the motor. As the CWW is fed and the wire melts, the arc rotates from t1 to t7 during each period of the welding process. This phenomenon is beneficial for transferring the heat at the center of the molten pool to both sides, thereby reducing the depth of penetration at the center of the weld.

The charged particles in the arc will rotate with arc rotation, as shown in Fig. 13. The liquid metal in the molten pool rotates regularly after interacting with the CWW arc; therefore, the heat distribution of the molten pool is even. This rotation not only allows the energy of the molten pool to flow to both sidewalls, thus not easily forming finger-shaped weld depths but also fully stirs the molten pool. Moreover, this mechanism produces fine grains in the weld microstructure, helping to improve weld performance, which is consistent with the weld performance test results.

Fig. 14 Geometric parameters of the CWW

Fig. 15 Schematic showing the trajectory of droplet movement. (**a**) At the edge of the molten pool. (**b**) Into the middle of the molten pool. (**c**) Outside of the molten pool
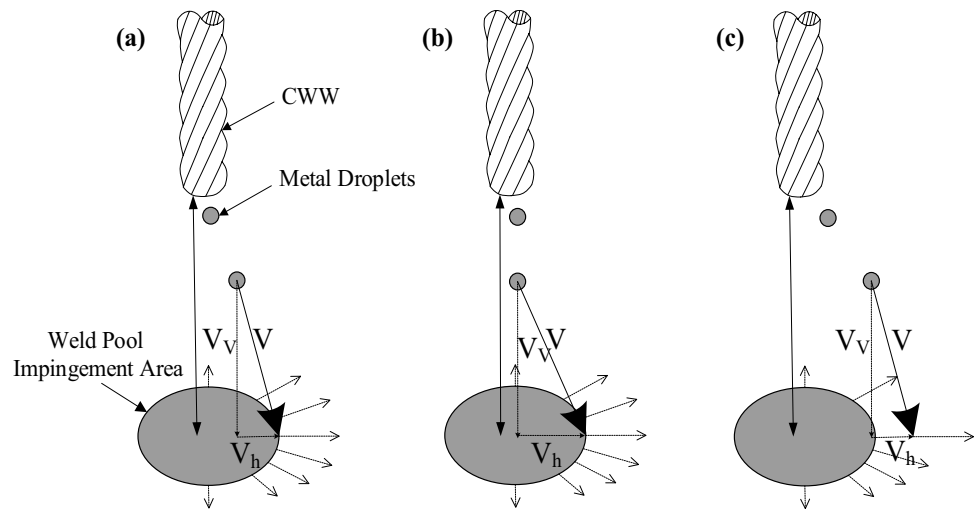
CWW NG-GMAW arc rotation is mainly related to the spiral angle, pitch, wire feed speed, and other factors. The geometrical parameters of CWW are shown in Fig. 14. Each twist of a wire in the CWW has a helix angle in regard to the center wire, and this angle extends along the wire between the wire tip and molten pool, which makes the twisted wire and molten pool have a certain angle. The larger the range of the effect is, the greater the area of effect on the molten pool with an increasing angle. The stirring action on the molten pool during CWW NG-GMAW increases with an increasing welding current, and CWW NG-GMAW exhibits a stronger stirring effect on the melting pool than single-wire GMAW.

2. Droplet transfer trajectory

Due to the CWW arc rotation behavior, the droplet remains in a certain rotation movement before transfer to the molten pool. Rotating forces still exist on the droplet after the droplet transfers to the molten pool, which stirs the molten pool and transfers heat to the sidewall. The droplet transfers to the molten pool in three possible modes, namely, falling into the center of the molten pool, outside of the molten pool, and away from the molten pool, as shown in Fig. 15. Guo et al. [26] reported that the rotating arc process could improve metal transfer, and the rotating force had a

Fig. 16 Schematic rotation frequency of CWW

large effect on the transfer model and droplet size. CWW droplets transfer into the center of the molten pool and at the edge of the molten pool, and their rotational force is converted into regular rotational motion in the molten pool and the oscillation of the melting pool.

The droplets fall away from the molten pool when the welding current is small, which produces a certain amount of splashing and results in a loss of deposited metal, as shown in Fig. 15a, c. The rotational force of the droplet is mainly related to the CWW feeding speed. That is, the current will increase with the CWW feeding speed, and the rotational force of the droplet will increase with the increasing welding current. The droplet transfers into the middle of the molten pool, as shown in Fig. 15b. The droplet transfer plays an important role in sidewall penetration, the droplet transferred at the edge of the molten pool will increase the sidewall penetration. It was due to the heat of droplet transferred to the sidewall, which could increase the sidewall penetration in the CWW NG-GMAW.

3. Molten pool movement

The flow of the molten pool during CWW NG-GMAW is mainly affected by the welding arc and droplet transfer. The molten pool exhibits a certain regular rotation from the analysis of the arc and droplet transfer during CWW NG-GMAW. Figure 16 shows a schematic of the CWW rotation frequency. The rotational movement of the molten pool depends on the rotational frequency (f_ω) of the CWW, the rotating frequency can be expressed by formula (8)

$$f_\omega = \frac{V}{2\pi D \tan\alpha} \tag{8}$$

where V is the wire feeding speed; D is the single-wire diameter; α is the helix angle of CWW; and f_ω is the rotation frequency.
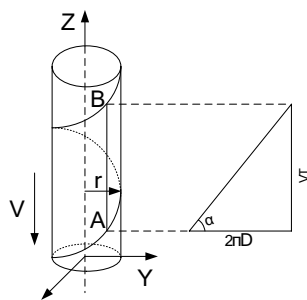
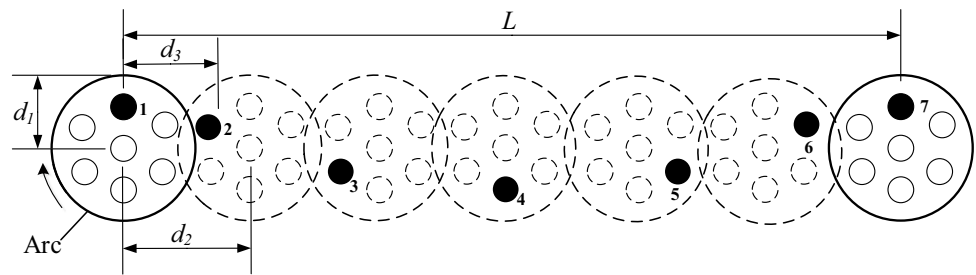**Fig. 17** Schematic showing the rotation of the peripheral wire
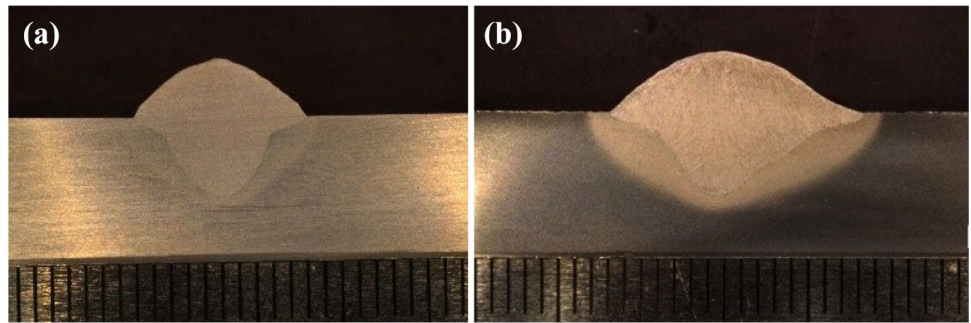

Fig. 18 Comparison of the weld cross sections produced by different welding methods. (**a**) Single-wire GMAW. (**b**) CWW GMAW (I = 460 A, U = 36 v)

From Fig. 16 and formula (8), it can be seen that the rotation frequency of the molten pool is consistent with the rotation frequency of the CWW. The moving position of a single wire in the CWW relative to the molten pool during CWW NG-GMAW is shown in Fig. 17. The rotational motion of the molten pool is consistent with the movement position of a single wire, which is relative to the flow of the molten pool. The role of the peripheral wire is consistent throughout the welding process; it moves from position 1 to 6, making the molten pool flow the welding process. The distance of L is affected by the welding speed and welding current. The rotational motion caused by the peripheral welding wire has an effect on the stirring and heat transfer of the molten pool, which improve sidewall penetration at the weld joint.

Figure 18 shows the weld cross sections of single-wire GMAW and CWW GMAW, respectively. The cross section formed in both method without pores, cracks, slags or other defects. However, CWW GMAW results in a weld with a greater width and higher deposition compared with single-wire GMAW. The ratio of width and penetration in CWW GMAW is smaller than single-wire GMAW under the same parameters. It is obviously to see that the CWW GMAW is beneficial to transfer the heat to the weld width direction, which is beneficial to obtain good sidewall penetration. Although these phenomena have been observed in the welding process, the driving force of the molten pool during the welding process is the main reason.

The flow force of the molten pool during CWW NG-GMAW is shown in Fig. 19. The speed changes at different positions in the molten pool. The flow speed in the molten pool is composed of the rotational speed and welding speed. The resultant speed at position C is greater than that at other positions. The flow speed in the molten pool at positions B and D affects sidewall penetration. Due to the molten pool flow characteristics, the width at the bottom of the molten pool increases, which reduces the effect of finger-shaped weld depths in the molten pool. Because the molten pool flow changes due to the force changes during the welding process, the major forces acting on the molten pool are beneficial to the molten pool flowing to both sidewalls, which is consistent with the conclusion of Xu et al. [10]. Therefore, the heat transfer benefits obtaining good sidewall penetration during CWW NG-GMAW.
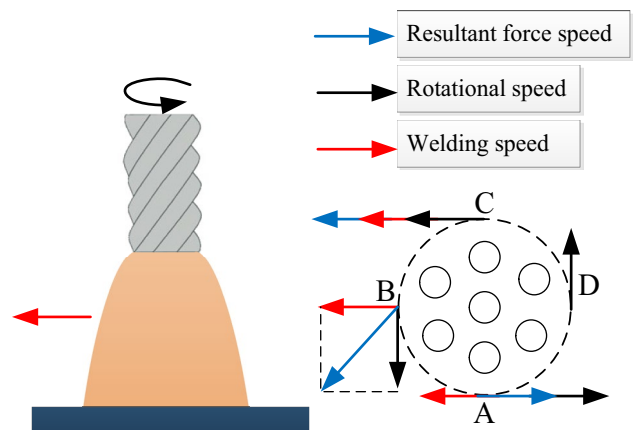

Fig. 19 Schematic showing the arc rotation process during CWW GMAW

4 Conclusion

From the above analysis, the following conclusions of CWW NG-GMAW can be drawn:

1. A self-rotating arc narrow gap welding method was established using cable-type welding wire. The mechanical property results demonstrated that the CWW NG-GMAW method could obtain an excellent shape and no defect welds, meeting the standard requirements.

2. Due to the unique structure of CWW, the wire melting and deposition speed of CWW GMAW increased by more than 20% compared with those of the single-wire GMAW. The surface area of CWW was 4.6 times that of a single wire when both had the same diameter. The resistance heat of 2.4 mm CWW GMAW was 1.45 times greater than that of single-wire GMAW at the same parameters.

3. The rotating arc played an important role in the sidewall penetration behavior caused by the self-rotation of the wire during the welding process. The impact of the droplet transfer trajectory on the molten pool helped improve heat transfer to the sidewall. The formation of the molten pool was affected by the rotating arc and droplet transfer, which benefitted heat transfer to the sidewall. The mechanical properties were consistent with the effect of the sidewall penetration behavior during CWW NG-GMAW.

4. The combined rotation arc and droplet transfer forces acting on the molten pool during CWW NG-GMAW were beneficial for total heat transfer to the sidewall and throughout the molten pool, thereby reducing the occurrence of finger-shaped weld depths and deeper sidewall penetration when compared to single-wire GMAW at the same welding parameters.

Author contribution Zhidong Yang: manuscript writing, editing; Yuntao Chen: data analysis; Zewei Zhang: investigation; Chenfu Fang: methodology, supervision; Kai Xu: visualization; Peng He: manuscript revising. Zhengdong Zhang: data curation.

Data availability The data associated with the article cannot be shared at this time as these are part of ongoing research work.

Declarations

Ethics approval Not applicable.

Consent to participate The authors in this article have informed consent to participate in this work.

Consent for publication The authors agree to publication in The International Journal of Advanced Manufacturing Technology.

Conflict of interest The authors declare no competing interests.

References

1. Ikram A, Raza A, Chung H (2020) Investigation of single pass welding of thick AH36 steel plates in a square groove butt joint configuration during AC-GMAW. Journal of Welding and Joining 38(3)

2. Andreazza P, Gericke A, Henkel KM (2021) Investigations on arc brazing for galvanized heavy steel plates in steel and ship-building. Welding in the World 65:1199–1210

3. Liu X, Dong Q, Wang P (2021) Review of electron beam welding technology in space environment. Optik- International Journal for Light and Electron Optics 225(11):165720

4. Xu Y, Ke L, Ouyang S (2021) Precipitation behavior of intermetallic compounds and their effect on mechanical properties of thick plate friction stir welded Al/Mg joint. J Manuf Process 64:1059–1069

5. Santini FF, Plaine AH, Afonso CR, Bergmann L, Miyazaki MH (2020) Microstructure features and mechanical properties of double-sided friction stir welded joints of aa2050-t84 thick plates. Mater Res 23(6)

6. Chen H, Feng S (2018) Application of welding and cutting equipment in high efficiency welding of engineering manufacturing. Henan Science and Technology 649(8):44–45

7. Wang J, Ren Y, Yang F, Guo H (2007) Novel rotation arc system for narrow gap mag welding. Sci Technol Weld Joi 12(6):505–507

8. Guo N, Lin S, Zhang, L, Yang, C (2009) Metal transfer characteristics of rotating arc narrow gap horizontal gmaw. Sci Technol Weld Joi 14(8):760–764

9. Cui HC, Jiang ZD, Tang XH, Lu FG (2014) Research on narrow-gap GMAW with swing arc system in horizontal position. Int J Adv Manuf Technol 74(1–4):297–305

10. Xu G, Li L, Wang J, Zhu J, Li P (2018) Study of weld formation in swing arc narrow gap vertical GMA welding by numerical modeling and experiment. Int J Adv Manuf Technol 96(5):1905–1917

11. Jones LA, Eagar TW, Lang JH (1999) A dynamic model of drops detaching from a gas metal arc welding electrode. J Phys D Appl Phys 31(1):107

12. Cai X, Fan C, Lin S, Yang C, Ji X, Hu L (2017) Effects of shielding gas composition on arc characteristics and droplet transfer in tandem narrow gap GMA welding. Sci Technol Weld Joi 22(5):446–453

13. Zhu C, Tang X, He Y (2018) Effect of preheating on the defects and microstructure in NG-GMA welding of 5083 Al-alloy. J Mater Process Technol 251:214–224

14. Li W, He C, Chang J (2020) Modeling of weld formation in variable groove narrow gap welding by rotating GMAW. J Manuf Process 57:163–173

15. Liu G, Tang X, Xu Q, Lu F, Cui H (2021) Effects of active gases on droplet transfer and weld morphology in pulsed-current NG-GMAW of mild steel. Chinese Journal of Mechanical Engineering 34(1)

16. Li J, Liu Y, Kang K, Sun Q, Jin P, Liu Y, Cai C, Sun Q (2020) A novel approach to regulate energy allocation and melt flow in narrow gap laser welding with electromagnetic assisted wire wobbling. J Mater Process Technol 289

17. Fang C, Chen F, Z, Xu G, Hu Q, Zhou H, Shi Z (2012) Study on the process of CWW CO_2 gas shielded welding. Acta Metall Sin 48(11):1299–1305

18. Yang Z, Fang C, Wu M (2018) The mechanisms of arc coupling and rotation in cable type welding wire CO_2 welding. J Mater Process Technol 255:443–450

19. Waqas A, Qin X, Xiong J, Zheng C, Wang H (2019) Analysis of ductile fracture obtained by Charpy impact test of a steel structure created by robot-assisted GMAW-based additive manufacturing. Metals - Open Access Metallurgy Journal 9(11):1208

20. Vasconcelos C, Loayza C, Assuno P, Junior F, Braga EM (2019) High-hardness armor welded by CW-GMAW: economic, geometric and CGHAZ analysis. J Braz Soc Mech Sci Eng 41(6)

21. Lambang F, Tamjidillah M (2020) Analysis of protective gas flow and seam formation on GMAW weld process to hardness and micro structure of ASTM a36 steel. Scientific Journal of Mechanical Engineering Kinematika 5(1):51–66

22. Han B, Zou Z, Qu SY (2006) Melting characteristic of twin electrode single arc welding I.Heating and melting of twin electrode. Transactions of the China Welding Institution 27(3):81–85

23. Modenesi PJ (2007) A model for melting rate phenomena in GMA welding. J Mater Process Technol 189:199–205

24. Tusek J (1999) A mathematical model for the melting rate in welding with a multiple-wire electrode. J Phys D Appl Phys 32(14):1739

25. Ueyama T, Ohnawa T, Tanaka M (2007) Occurrence of arc interaction in tandem pulsed gas metal arc welding[J]. Sci Technol Weld Joi 12(6):523–529

26. Guo N, Lin SB, Zhang L, Yang CL (2009) Metal transfer characteristics of rotating arc narrow gap horizontal GMAW. Sci Technol Weld Joi 14(8):760–764